LEVEL III

A055936

EPITAXIAL GROWTH OF SEMI-INSULATING GaAs

RCA Laboratories
Princeton, New Jersey 08540

S. T. Jolly, C. P. Wu
D. S. Vaney, S. Y. Narayan
S. G. Liu

ANNUAL REPORT,
~~for period~~ 1 July ~~1977~~ to 30 June ~~1978~~

May 78 | 57 p. | PRRL-78-CR-38

Sponsored by
Defense Advanced Research Projects Agency (DOD)
Arlington, Virginia 22209

DARPA Order No. 3441 BASIC
Program Code No. 7D10

Monitored by
Office of Naval Research
Arlington, Virgina 22217
Under Contract No. N00014-77-C-0542; DARPA Order-3441

DARPA-3441
7D10

UNCLASSIFIED

SECURITY CLASSIFICATION OF THIS PAGE (When Data Entered)

REPORT DOCUMENTATION PAGE		READ INSTRUCTIONS BEFORE COMPLETING FORM
1. REPORT NUMBER	2. GOVT ACCESSION NO.	3. RECIPIENT'S CATALOG NUMBER
4. TITLE (and Subtitle) EPITAXIAL GROWTH OF SEMI-INSULATING GaAs		5. TYPE OF REPORT & PERIOD COVERED Annual Report (1 July 1977 to 30 June 1978) 6. PERFORMING ORG. REPORT NUMBER PRRL-78-CR-38
7. AUTHOR(s) S. T. Jolly, D. S. Yaney, S. G. Liu, C. P. Wu and S. Y. Narayan		8. CONTRACT OR GRANT NUMBER(s) DARPA Order No. 3441 BASIC Program Code 7D10 N00014-77-C-0542
9. PERFORMING ORGANIZATION NAME AND ADDRESS RCA Laboratories Princeton, New Jersey 08540		10. PROGRAM ELEMENT, PROJECT, TASK AREA & WORK UNIT NUMBERS PE 61101E/Program Code 7D10/NR 243-018
11. CONTROLLING OFFICE NAME AND ADDRESS Defense Advanced Research Projects Agency (DOD) 1400 Wilson Boulevard Arlington, Virginia 22217		12. REPORT DATE March 1978 13. NUMBER OF PAGES 51
14. MONITORING AGENCY NAME & ADDRESS (if different from Controlling Office) Office of Naval Research Arlington, Virginia 22217		15. SECURITY CLASS. (of this report) Unclassified 15a. DECLASSIFICATION/DOWNGRADING SCHEDULE N/A

16. DISTRIBUTION STATEMENT (of this Report)

Approved for public release; distribution unlimited.

17. DISTRIBUTION STATEMENT (of the abstract entered in Block 20, if different from Report)

18. SUPPLEMENTARY NOTES

ONR Scientific Officer
Telephone: (202) 696-4218

19. KEY WORDS (Continue on reverse side if necessary and identify by block number)

Semi-insulating (SI) GaAs
Epitaxial growth
Photoconductive (PC) response
Chromium doping
Buffer layers
Photoelectronic methods
Ion implantation

20. ABSTRACT (Continue on reverse side if necessary and identify by block number)

This report describes the work performed during the first twelve months of a research program to develop techniques for the epitaxial growth of high resistivity GaAs to be used in the fabrication of planar devices such as field effect transistors. The original reactor design has been modified to improve reproducibility of results, and permit the use of chromyl chloride as a dopant. Epitaxial layers with resistivities greater than 10^5 Ω-cm and point contact breakdown voltages

DD FORM 1 JAN 73 1473

UNCLASSIFIED

SECURITY CLASSIFICATION OF THIS PAGE (When Data Entered)

20.

higher than 1500 V were grown. Device wafers incorporating these layers have been grown.

In the area of material characterization, various methods, analytical, electrical, and optical, were employed, both for the evaluation of semi-insulating substrates from different vendors and also in the attempts to evaluate the thin, high resistivity epi-layers grown during the program.

Preliminary work on the suitability of the high resistivity epitaxial layers for application to ion implantation has been carried out. Our results indicate that implantation into such layers gives more consistency and superior mobility for a given carrier concentration than most bulk high resistivity GaAs substrates.

PREFACE

This annual report describes research done in the Microwave Technology Center of RCA Laboratories during the period 1 July 1977 to 30 June 1978 in a program sponsored by Defense Advanced Research Projects Agency (DOD) under DARPA Order No. 3441 BASIC and monitored by the Office of Naval Research under Contract No. N00014-77-C-0542. F. Sterzer is the Center's Director; S. Y. Narayan is the Project Supervisor, and S. T. Jolly is the Project Scientist. D. S. Yaney carried out the materials characterization effort. The ion implantation research was carried out by S. G. Liu and C. P. Wu.

TABLE OF CONTENTS

LIST OF ILLUSTRATIONS

LIST OF ILLUSTRATIONS (Continued)

LIST OF TABLES

SECTION I

INTRODUCTION

The objective of the program is to develop techniques for the vapor phase growth of high resistivity epitaxial layers of GaAs on semi-insulating (SI) GaAs substrates. A capability to grow high resistivity buffer layers with minimum structural defects prior to the growth of active device layers would eliminate device performance problems caused by poor and inconsistent substrate quality.

During the program a reactor and its associated gas handling system was built. Both undoped and chromium doped high resistivity epitaxial layers were grown with excellent surface morphology.

In order to determine the properties of the material grown, a parallel effort in material characterization has been carried out. This effort has included measurement of electrical and photoconductive properties as well as the employment of various analytical techniques to determine the concentrations of chromium introduced during the material growth.

In addition to the above work, the quality of the semi-insulating epitaxial layers has been assessed and compared with bulk material by ion implantation of ^{32}S and ^{28}Si into both the epi-layers and bulk chrome doped wafers. It has been shown that the n-layers generated in the vapor phase grown layers has greater consistency and higher electron mobility than those formed in the bulk material for a given carrier concentration.

SECTION II

MATERIAL GROWTH

A. INTRODUCTION

The success of planar devices such as GaAs field-effect transistors (FETs) and transferred-electron logic devices (TELDs) depends on the capability of growing thin ($\leq$ 1.5 μm) high-quality n-layers on substrates which are "inert" (i.e., they do not affect the electrical and mechanical properties of thin layers grown epitaxially on them). A major problem is the present unreliability of available substrate material. A possible solution which this program proposes to investigate is the growth of a high-quality semi-insulating buffer layer with good surface morphology, high electrical resistivity, and the minimum of interaction with the active n-layer subsequently grown on it. This report presents the results obtained in the first year of a program to develop techniques for the epitaxial growth of high resistivity GaAs layers. Some of the results were described earlier in a semiannual report [1].

B. BACKGROUND

This section describes the state of the art at the inception of this program. In a previous company-sponsored effort, we have established the feasibility of the epitaxial growth of chromium-doped semi-insulating (SI) GaAs, using CrO_2Cl_2 as the doping gas. This study established the following:

1. For chromium doping with CrO_2Cl_2 to be effective, the background donor density in the reactor must be $\leq 2 \times 10^{15}\ cm^{-3}$.

2. When the background donor density is in the required range, chromium-doped SI GaAs layers can be grown. The point-contact-breakdown voltage of such epi-SI GaAs layers is in excess of 1500 V. Measurements carried out on these layers at the USAF Avionics Laboratory indicate a resistivity in the 10^6-10^7-Ω-cm range.

3. The surface morphology of the chromium-doped epi layers was poor compared to that of epi n layers. The reason for this poor morphology was not well understood. Careful adjustment of the CrO_2Cl_2 gas flow resulted in some minor improvement.

4. The CrO_2Cl_2/H_2 dopant mixture decomposed in the feed tube, and the resulting deposit clogged the tube. It was presummed that the H_2 in the mixture reduced CrO_2Cl_2 in the hot part of the feed tube.

5. The 500-ppm $CrO_2Cl_2H_2$ mixture was then replaced by a 500-ppm CrO_2Cl_2/He mixture. This greatly minimized the decomposition in the feed tube. Furthermore, lower flow rates of the CrO_2Cl_2/He mixtures could be used to obtain SI GaAs. The surface quality also improved slightly. The point-contact breakdown of the grown layers was again in excess of 1500 V.

One chromium-doped epitaxial GaAs layer was evaluated at the USAF Avionics Laboratory, Dayton, Ohio. In one experiment, a (100) oriented slice from a bulk-grown SI GaAs substrate was cut into two pieces. On one, a 5-μm-thick epitaxial chrome-doped layer was grown, and the other was used as a control sample. At the Avionics Laboratory, the electron-and-hole concentration, mobility, and IR photoconductivity at 4.2 K were measured. Table 1 and Fig. 1 illustrate the results. The superior properties of the epi-SI layer are evident.

TABLE 1. DATA TAKEN BY USAF AVIONICS LABORATORY, DAYTON, OHIO

	Type	Resistivity (ohm-cm)	$n\text{-cm}^{-3}$	$p\text{-cm}^{-3}$	μ_n ($cm^2/V\cdot s$)	μ_p ($cm^2/V\cdot s$)
Substrate	n	7.11×10^7			1041	
Epitaxial buffer layer	n	7.09×10^7	1.65×10^7	1.58×10^8	4202	403

The resistivity of the epi layer is 10^7 ohm-cm. Figure 1 shows that the photoconductive response of the epi layer is much sharper than that of the substrate. This is believed to be indicative of superior crystal quality.

In the final analysis, the best measure of material quality is the performance of an active device fabricated from it. n^+-n-n_B(Buffer)-Si GaAs wafers were grown *in situ* for power FET fabrication; n_B denotes an epitaxial SI GaAs buffer layer. The buffer-layer thickness was about 5 μm. FETs of 1.5-μm gate length were fabricated from this wafer. Table 2 summarizes the results obtained. *Note that excellent performance was obtained from a FET*

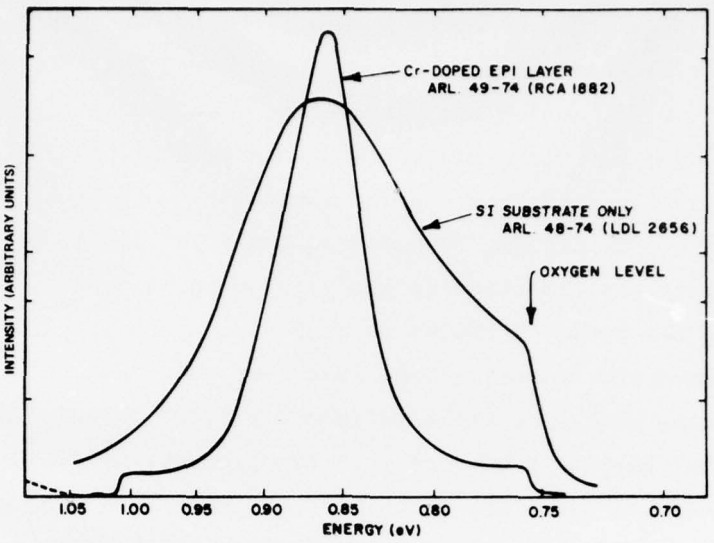

Figure 1. Photoconductivity response of bulk Cr-doped substrate and epitaxial Cr-doped buffer layer. Measurement made at AFAL, Dayton, Ohio.

TABLE 2. RCA GaAs FET PERFORMANCE (WITH CHROME-DOPED BUFFER LAYER)

Frequency (GHz)	Linear Gain (dB)	Output Power (mW)	Gain at P_{out} (dB)	Power-Added Efficiency (%)	Operating Condition (Source Periphery)
9	5.5	1000	4.3	16.3	Class A (1800 μm)
15	6.7	451	5.2	12.5	Class A (1200 μm)
18	6.3	225	4.5	5.4	Class A (1200 μm)
21	5	186	4.3	11.9	Class A (600 μm)
22	5.6	141	4.8	9	Class A (600 μm)

with 1.5-μm *gate length at frequencies as high as 22 GHz* [2]. These data indicate that the n layer grown on an epi-SI buffer layer has excellent electron-drift mobility. These results are far superior to those obtained from 0.8-μm-gate FETs fabricated from n layers grown directly on bulk-grown SI GaAs substrates.

We have also fabricated planar transferred-electron logic devices (TELDs) from a wafer with an epitaxial SI GaAs buffer layer. Post-threshold current drops as high as 28% were obtained with three terminal TELDs; this, again, is

indicative of higher electron-drift mobility in n layers grown on epitaxial SI GaAs layers.

While the feasibility of growth of SI GaAs layers by vapor-phase epitaxy (VPE) and its impact on planar GaAs devices has been established, further research work was necessary to improve the reproducibility of the growth process. The following problem areas had to be addressed.

1. For the improvement of surface morphology, the occurrence of microscopic pitlike defects must be eliminated. This is necessary to obtain submicrometer line lengths and features required for microwave and multigigabit-rate logic circuits. The reasons for the occurrence of these imperfections was not understood.

2. Optimum conditions for reproducible and repeatable growth of SI GaAs layers have to be established.

3. The use of metallic Cr and its transport by Cl_2 gas may eliminate the need for CrO_2Cl_2, which is highly toxic. This needs to be investigated.

4. Researchers at Fujitsu in Japan have established that the use of metallic Fe and its transport to the substrate as $FeCl_2$ can result in high-resistivity Fe-doped GaAs [3]. They report excellent FET results from wafers with Fe-doped buffer layers. Fe-doped GaAs with resistivities as high as 10^5 Ω-cm have been achieved. Fe-doped high-resistivity layers should also be studied.

C. REACTOR DESCRIPTION

The vapor-phase reactor in which the original experiments were carried out was modified to make it more suitable for this particular program. Figure 2 shows the schematic of the redesigned gas-handling system. This system has the following characteristics:

1. Ability to operate as a "normal" $Ga/Cl_2/AsH_3$ system employing palladium-diffused hydrogen as the diluting gas. It is also planned to add the ability to substitute ultrapure nitrogen for the hydrogen. This will be of significance in attempts to employ metallic chromium or iron as the doping element.

2. A third input line was added to the reactor to allow the introduction of chromyl chloride/helium mixture of variable composition.

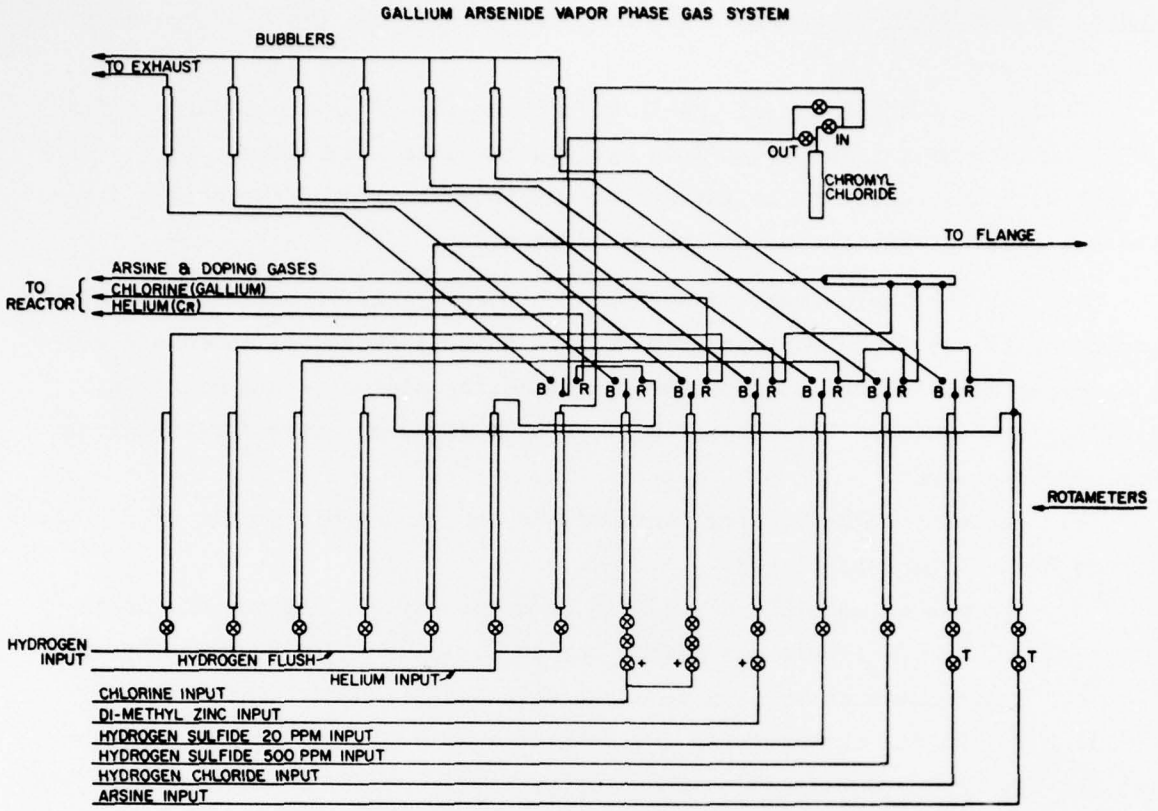

Figure 2. Schematic diagram of reactor gas-handling system.

3. An HCl feed was added to the arsine/hydrogen line to allow a mixture of hydrogen chloride to the reactant gases downstream of the gallium boat to determine the effect of HCl partial pressure on growth rate, background carrier concentration, etc. This HCl was also used to etch clean the reactor tube and substrate holder prior to deposition runs.

4. n-type doping gases such as hydrogen sulfide, hydrogen selenide, or hydrogen telluride could be introduced.

5. Inclusion of a line for addition of other doping materials such as diethylzinc to allow p-type doping.

6. An ability to introduce chlorine into the chromium doping line. The use of metallic chromium or iron in the chromium feed tube of the reactor permits the addition of the respective metallic chlorides into the reacting gas stream. This could be a considerably safer and more convenient method of adding chromium than the use of chromyl chloride.

Figure 3 is a schematic diagram of the reactor tube and furnace assembly. The reactor tube configuration has been changed from that previously employed

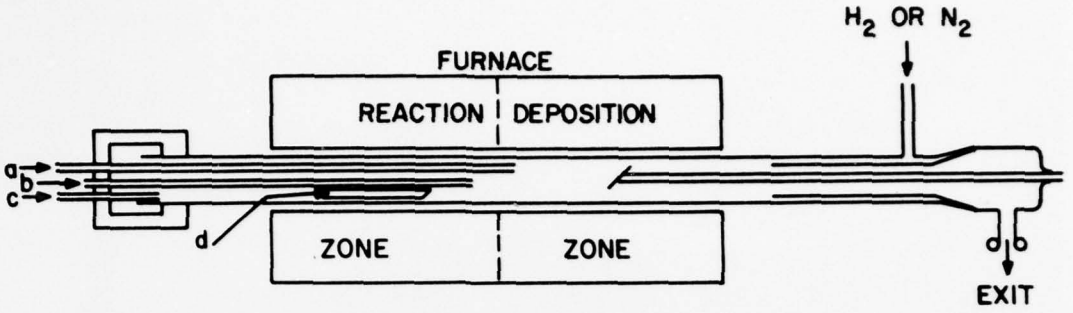

a CHROME TUBE
b AsH_3 TUBE
c Cl_2 OR HCl TUBE
d GALLIUM BOAT

Figure 3. Schematic diagram of reactor tube/furnace assembly.

at RCA for vapor deposition of GaAs by the Ga/HCl/AsH_3 system. The sidearm previously used to discharge the waste products of the system has been eliminated.

The reactor now consists of a single straight quartz tube. The exit end of the tube is closed by an end cap with a sleeve extending so far up the reactor tube that sliding the furnace down the tube permits it to be heated and etched clean of reaction products. A small quantity of hydrogen or nitrogen flows slowly upstream between the reactor tube and the sleeve; this restricts reaction products to the interior of the sleeve and prevents their deposition on the walls of the reactor tube downstream of the end of the sleeve. The substrate holder is incorporated in the end-cap holder-sleeve assembly and extends beyond the end of the sleeve into the deposition region of the reactor. Figure 4 is a photograph of the reactor.

The elimination of the sidearm achieves several objectives:

1. It eliminates the necessity to dismantle the assembly to remove the reactor tube for cleaning whenever the performance of the reactor is affected by the deposits of reaction products in a sidearm.

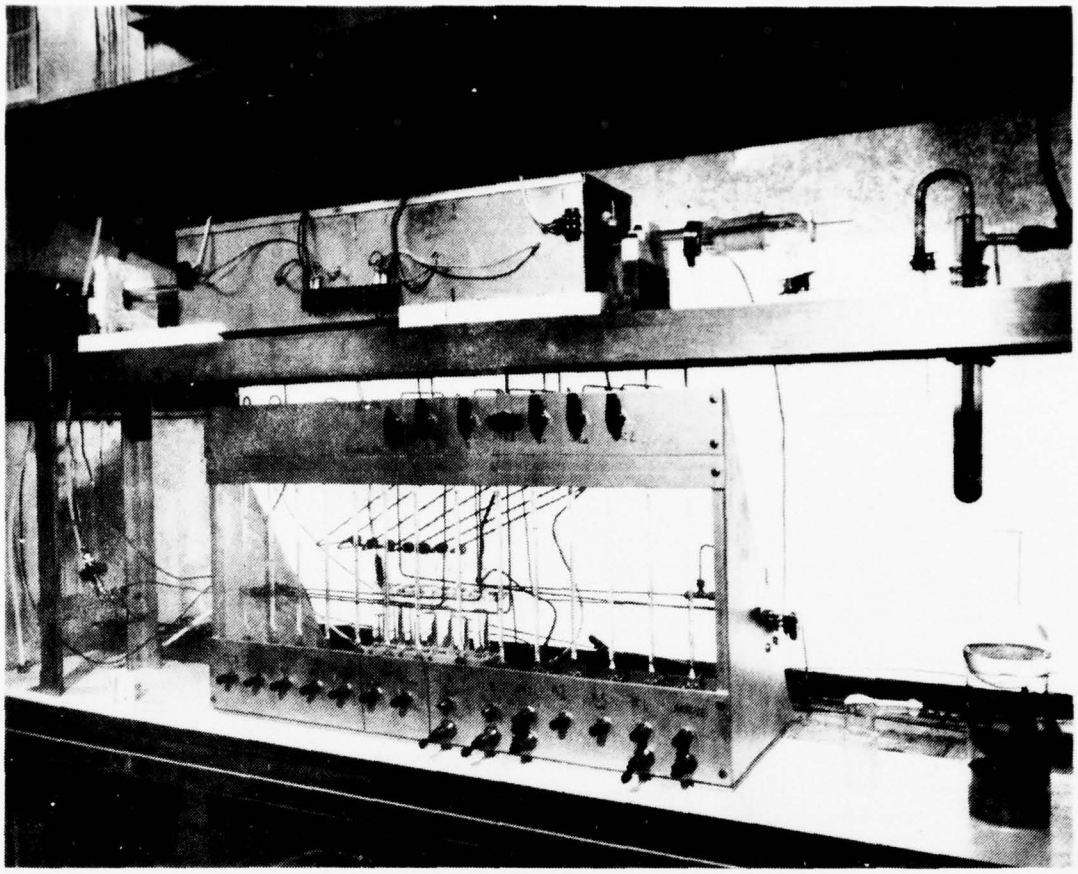

Figure 4. Photograph of reactor.

2. It reduces the history effect (i.e., change in the background impurity level produced after growth of highly doped layers). This feature is important when attempting to grow a buffer layer after a highly doped device wafer has been grown.

3. The reactor tube can be etch cleaned (with hydrogen chloride gas) before every run without dismantling the system.

4. The gas flow pattern is uniform down to the tube and is not affected by the reverse gas flow from the loading end of the reactor, required to force the reaction products down the side exit arm.

Other features of the reactor assembly are the employment of a sapphire feed tube for the introduction of the chromyl chloride/helium mixture into the reaction zone, the use of a pyrolytic boron nitride sleeve to protect the reactor tube from attack by the chromyl chloride in the reaction zone, and the

employment of an annular heat pipe using sodium as the heat transfer medium as a heating device for the deposition zone.

D. RESULTS

1. Undoped High-Resistivity Layers

The reactor has been fabricated and is now operational. As discussed earlier, to obtain Cr-doped epitaxial SI layers, it is necessary to ensure that the reactor background is n type, and (N_D-N_A) is less than 2×10^{15} cm^{-3}. The initial wafers grown in the reactor were found to be of high resistivity even in the absence of added Cr. The reactor was completely leak checked to ensure that there was no oxygen or moisture present. Epitaxial layers were again grown on SI GaAs substrates. The epitaxial layers were found to be of high resistivity with $\rho > 3\times10^{4}$ Ω-cm at 300 K. The resistivity at 77 K was too high to measure. This indicates that the high resistivity is due to some deep level or levels. A sample was sent to our analysis group for evaluation by SIMS to determine whether it is due to a specific dopant or caused by defects. This test was inconclusive.

The occurrence of high-resistivity background layers during growth on high-resistivity substrates has been noticed before [4]. The experiments of Cox and DiLorenzo [4] indicate that this is due to the diffusion of acceptors from the substrate or the substrate-epi layer interface. In fact, Cox and DiLorenzo utilize this high-resistivity layer as a buffer layer for FETs [4]. We have observed such layers previously with the $AsH_3/Ga/Cl_2$ process. The nature of the acceptors is not known; it is suspected that they are point defects.

Attempts to characterize these undoped layers by the usual Van der Pauw methods have been made. Resistivities of the order of $4\text{-}5\times10^{4}$ ohm-cm have been measured. Attempts to determine carrier concentration from these experiments have failed due to insufficient equipment sensitivity. An improved Van der Pauw setup was developed and is described in Section III.C. However, with substrate/epi-layer thickness ratios of approximately 10 to 21, measurements are strongly influenced by the presence of the substrate.

A rough method, adopted for assessing the breakdown voltage of the epi layers, is as follows: Two tungsten wire probes are pressed onto the surface

of the epi layer, spaced approximately 0.25 cm apart, and a voltage is applied between them by means of a curve tracer. This gives an I/V curve and shows the voltage breakdown of the material, if any. Good buffer layers will withstand up to 1500 V, the maximum capability of the instrument. Figure 5 shows traces produced by wafers A94 and A95.

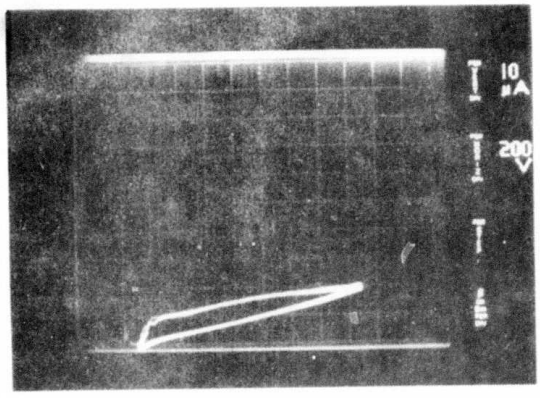

A94

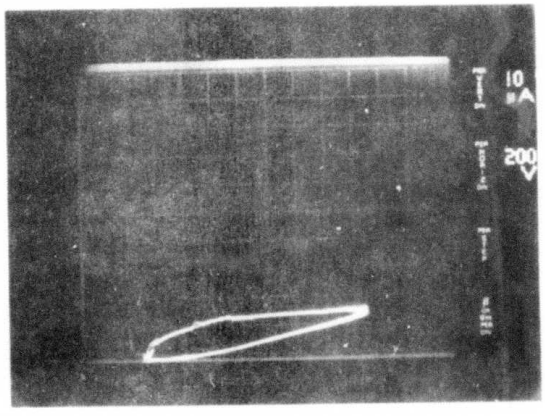

A95

Figure 5. Two-point probe characteristics of undoped layers.

2. Chromium-Doped Layers

The original method selected to attempt chromium doping was to bubble a carrier gas (helium) through liquid chromyl chloride. Because of a suspected leak in this part of the system, we are currently using a 500-ppm mixture of chromyl chloride (CrO_2Cl_2) in helium prepared in cylinders by Airco Precision Gas Co.*

Several chromium-doping runs have been made. Typical curve-tracer breakdown photographs are shown in Fig. 6. In Fig. 6, note that a dopant flow of 500 ml/min of CrO_2Cl_2 (500 ppm) produces a higher resistivity than does a flow of 275 ml/min. When the flow was increased to 1000 ml/min, the layer reverted to n-type with mid-$10^{14}cm^{-3}$ carrier concentration.

The surface morphology of Cr-doped layers grown in the modified reactor is excellent. This is in contrast to the layers grown in our older reactor. Possible explanations for this is the complete cleaning of the reactor with HCl prior to growing and the elimination of the sliding substrate feed rod.

3. Device Wafers

As the object of growing semi-insulating layers on SI GaAs substrates is to provide a superior surface for the growth of device wafers, a number of wafers suitable for GaAs FET fabrication have been grown. These have either a 12-μm-thick undoped high-resistivity layer or a chrome-doped layer, followed by the n and n^+ layers needed for FET fabrication. These wafers are A63, A67, A73, and A73 with undoped buffer layers, and A69 with a chrome-doped buffer layer. Figure 7 shows the carrier-concentration profile of wafer A69. After a few runs, several problems were encountered.

At a later point in the program, attempts to fabricate FET device structures by first growing a buffer layer followed by an n ($\sim 8\times10^{16}cm^{-3}$) and then an n^+ ($3\text{-}5\times10^{18}cm^{-3}$) layer produced results which have not yet been explained. This is illustrated in Fig. 8 by a carrier profile plot for wafer 151 produced by computation from conductivity versus thickness measurements. The effect appears to be that the growth of the n^+ or contact layer smears out the n-layer into the buffer layer in spite of the fact that the time required to grow the

*Riverton, NJ.

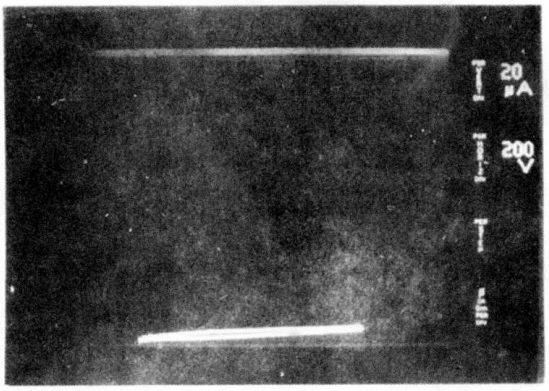

A89

Dopant flow:
500 ml/min.

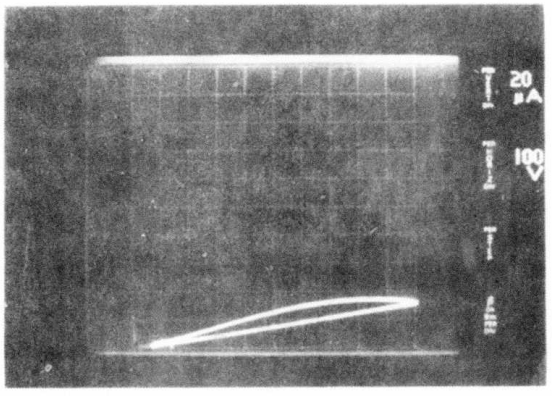

A92

Dopant flow:
275 ml/min.

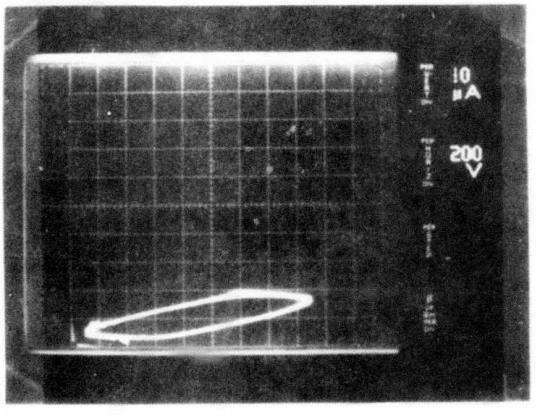

A96

Dopant flow:
500 ml/min.

Figure 6. Two-point-probe data for Cr-doped epi layers.

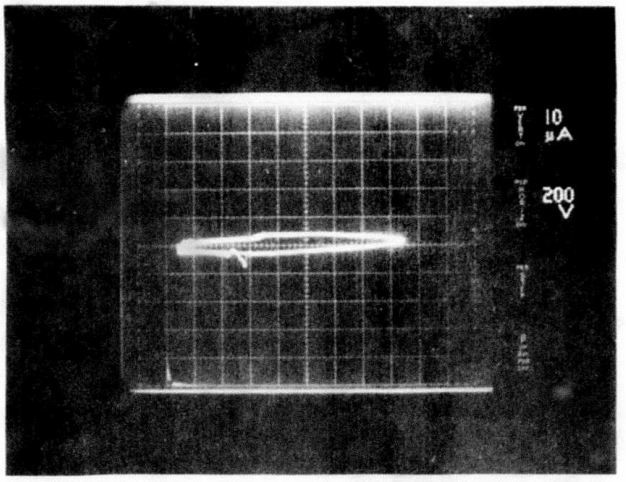

A141

Dopant flow:
500 ml/min

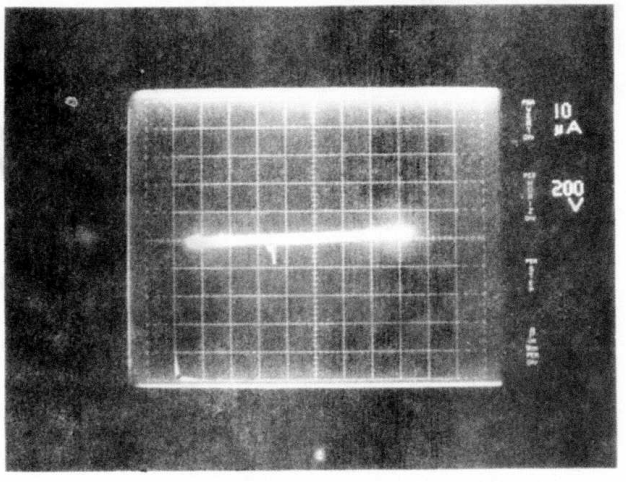

A156

Dopant flow:
250 ml/min

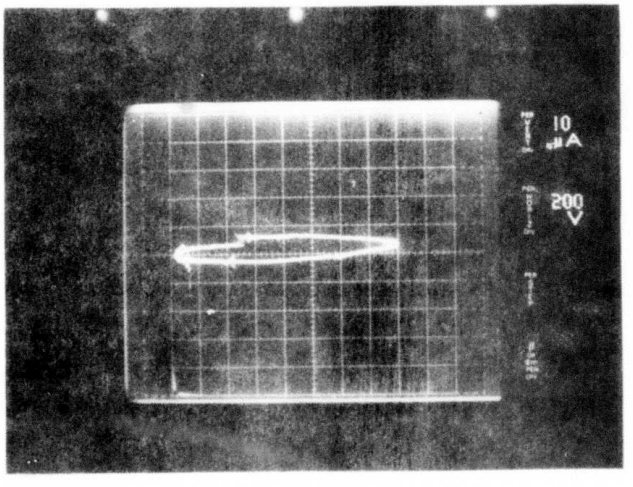

A173

Wafer placed on
PBN plate.
Dopant flow:
250 ml/min

Figure 6. Continued.

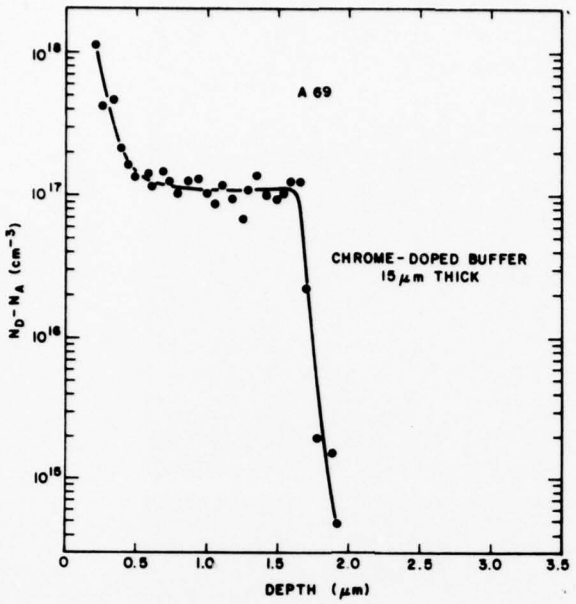

Figure 7. Carrier-concentration profile of wafer A69.

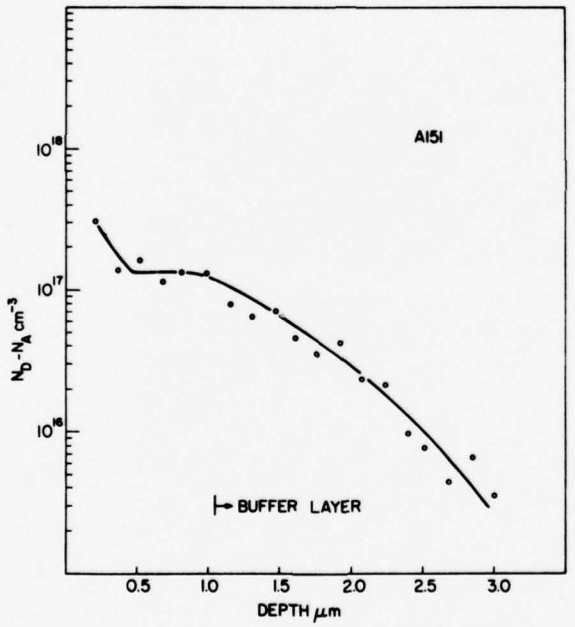

Figure 8. Carrier profile of A151 showing washed out buffer layer.

n^+ layer is only approximately a minute. This may be compared with results obtained from wafer 150 on which was grown a 1 μm layer on a thick Cr-doped buffer layer. Figure 9 is the profile produced by conductivity measurements

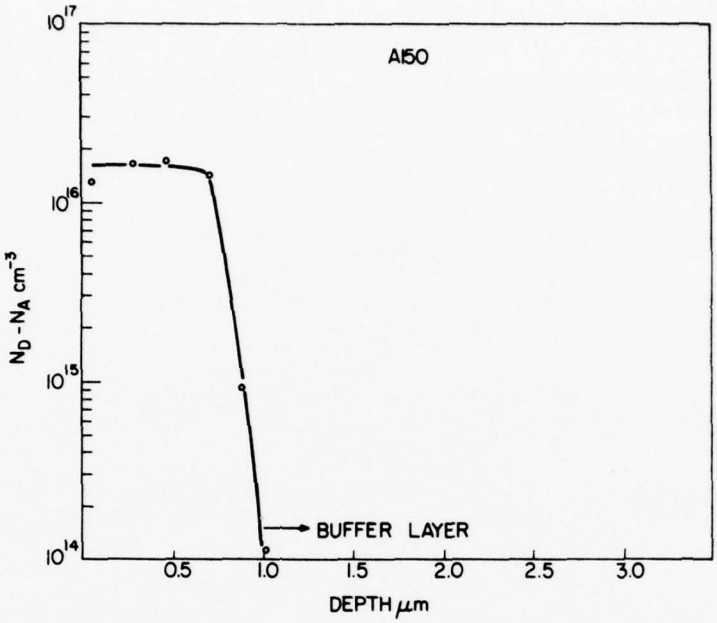

Figure 9. Carrier profile of A150 n-layer/buffer layer wafer deduced from conductivity measurements.

and Fig. 10 is a carrier profile plot from C/V measurements. After removing the n-layer, a carrier concentration in the buffer layer of approx. $2x10^{12}cm^{-3}$ was measured. Figure 11 (carrier profile plot of wafer 207) shows a similar sharp boundary between the n and buffer layers.

It was postulated initially that the substrate could be a source of carriers but this seems unlikely when buffer layers of $N = 2x10^{12}cm^{-3}$ and over 10 μm thickness have been interposed between the substrate and the n-layer. However, this experiment has been repeated with a number of different substrates with similar results. The result of another attempt to eliminate this apparent diffusion of the n-layer into the Cr-doped buffer when growing the n^+ contact layer is shown in Figs. 12 and 13 which are carrier profile plots obtained from wafers A189 and A190. In these runs, silane was used in place of H_2S as the doping gas for the n^+ layer. Although the n-layer/buffer layer interface is

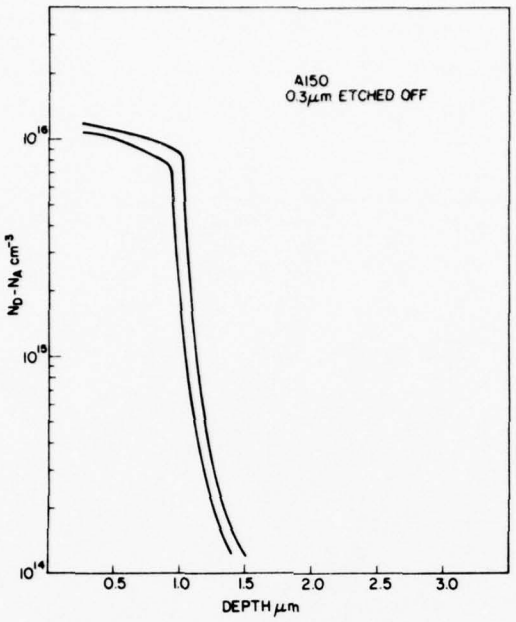

Figure 10. Carrier profile of A150 from automatic profile plotter (CV measurement).

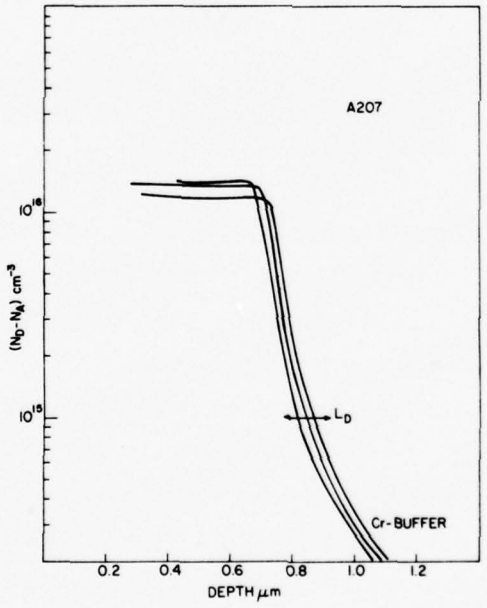

Figure 11. Carrier profile of n-buffer layer wafer. Note sharp boundary.

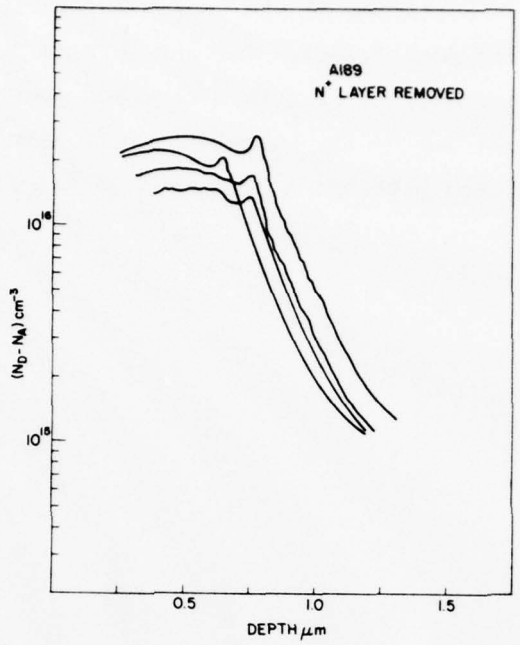

Figure 12. Profile of N^+-n-buffer layer wafer grown with silane.

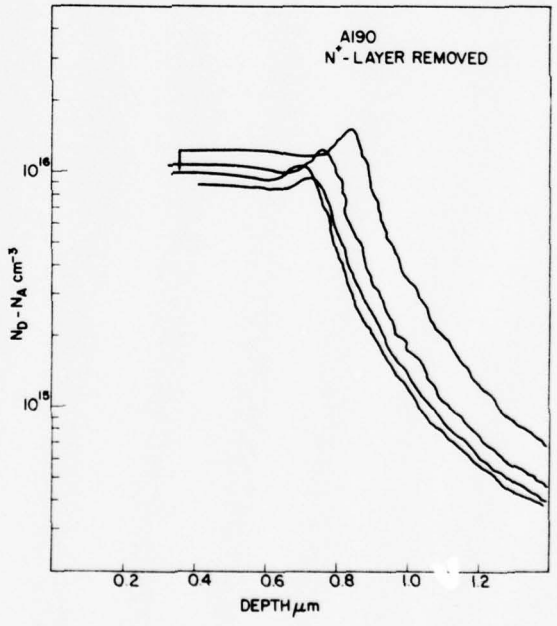

Figure 13. Profile of N^+-n-buffer layer wafer. N^+ layer grown using silane.

sharper, the carrier concentration of the buffer layer close to the interface still shows the effect to some degree. Further work on this question is required to determine the mechanism of this effect and overcome it.

Table 3 is a partial log of the wafers grown to illustrate typical results, growth sequence, tests, and problems encountered to date, during the course of the program.

TABLE 3. WAFER GROWTH RECORD (PARTIAL)

Run No.	Experiment	Substrate	Comments
A138	Cr-doping test CrO_2Cl_2 flow 500 ccpm	Morgan M1	Good high resistivity layer V_B > 1500 V. Note M1 substrate shows thermal conversion when annealed.
A139	Repeated 138, changed carrier gas from H_2 to N_2	Morgan M1	Very low growth rate, poor layer.
A140	Cr-doping test CrO_2Cl_2 flow 750 ccpm	NK 2715 (Nikkei Kako)	n-type layer, low $V_B \simeq 100$ V.
A141	Cr-doping test CrO_2Cl_2 flow 250 ccpm	NK 2715	Good high resistivity layer. V_B > 1500 V.
A142	Back doping test		Not relevant to program.
A143	n^+-n FET structure or Cr-doped buffer	NK 3115	Smeared profile.
A144	Repeat of 143	NK 3115	Smeared profile.
A145, A146	Aborted		Problems with chromium line.
A147, A148	Cr-doping test CrO_2Cl_2 flow 500 ccpm		Low breakdown woltage.
149	Cr-doping test CrO_2Cl_2 flow 500 ccpm		Good high resistivity layer V_B > 1500 V.
150	n-layer on Cr-doped buffer		Good sharp interface, buffer is high resistivity. See Figs. 9 and 10.

TABLE 3. (Continued).

Run No.	Experiment	Substrate	Comments
A151	n^+-n-Cr buffer FET structure		Smeared profile - See Fig. 8.
A152, A153	Repeat A151.		Smeared profile.
A154, A155			Tests not relevant to program goals.
A156	Cr-doping test CrO_2Cl_2 flow 250 ccpm		Good high resistivity layer, V_B > 1500 V.
A157	n-layer on Cr-doped buffer	NK 2912	Leak in wafer holder. Repaired after run.
A158	Repeat A157	NK 2912	Sharp interface: Hall data on n-layer $n(300) = 1.2 \times 10^{17} cm^{-3}$; $\mu(300) = 5200\ cm^2v^{-1}s^{-1}$ $n(77) = 8 \times 10^{16} cm^{-3}$; $\mu(77) = 11{,}900\ cm^2v^{-1}s^{-1}$. Very good mobility. So good that a slight conducting knee on buffer layer is suspected.
A159	Not relevant to program		
A160	n-layer on Cr-doped buffer		Sharp interface. Hall data on n-layer $n(300) = 5 \times 10^{16} cm^{-3}$; $\mu(300) = 5988\ cm^2v^{-1}s^{-1}$ $n(77) = 4.5 \times 10^{16} cm^{-3}$; $\mu(77) = 7138\ cm^2v^{-1}s^{-1}$.
A161	n^+-n-Cr-doped buffer FET structure	Metals Research A35	Smeared profile.
A162	n^+-n-Cr-doped buffer FET structure	Metals Research A35	Smeared profile.

TABLE 3. (Continued)

Run No.	Experiment	Substrate	Comments
A163	Reactor background test		$n(300) = 8 \times 10^{14} cm^{-3}$; $\mu(300) = 7612\ cm^2 v^{-1} s^{-1}$ $n(77) = 8.9 \times 10^{14} cm^{-3}$; $\mu(77) = 57,368\ cm^2 v^{-1} s^{-1}$. Good enough for Cr-doping to be effective.
A164-A166	Cr-doping tests		Poor results, low V_B.
A167	Reactor background test		$n(77) = 2 \times 10^{14} cm^{-3}$; $\mu(77) = 75,952\ cm^2 v^{-1} s^{-1}$. Should be good enough for Cr-doping; cannot explain problems with 164, 165 and 166.
A168	Cr-doping test		Holder leak problems.
A169	Background test		$n(300) = 7.3 \times 10^{14} cm^{-3}$; $\mu(300) = 7540\ cm^2 v^{-1} s^{-1}$. $n(77) = 7.7 \times 10^{14} cm^{-3}$; $\mu(77) = 61,832\ cm^2 v^{-1} s^{-1}$.
A170	Cr-doping test		Edges have low V_B, center is good.
A171	Repeat 170, interposed pyrolytic BN plate between wafer and quartz holder		Low V_B.
A172	Repeat A171		Good wafer with $V_B > 1500$ V.
A173	Repeat A171		Good wafer with $V_B > 1500$ V.
A174	Repeat A171		Breakdown voltage decreased to 100 V.
A175-A178	Other tests not relevant to program		
A179	Background test		$n(300) = 6.4 \times 10^{14} cm^{-3}$; $\mu(300) = 8271\ cm^2 v^{-1} s^{-1}$. $n(77) = 6.7 \times 10^{14} cm^{-3}$; $\mu(77) = 61,602\ cm^2\ -1\ -1$.

TABLE 3. (Continued)

Run No.	Experiment	Substrate	Comments
A180	Cr-doping test; CrO_2Cl_2 500 ccpm		Good layer, V_B > 1500 V.
A181	n-layer, Cr-doped buffer structure		Good sharp interface.
A182-A186	n^+-n-Cr doped buffer FET structure	NK2912	Smeared profiles.
A187	Repeat A186 but with no n^+-layer	Laser Diode LD9918	Sharp interface.
A188	Repeat A187; left wafer in reactor for 2 extra mins to simulate n^+-layer growth.		Sharp interface - No effect of extra 2 minutes observed.
A189, A190	Repeat A186 but used SiH^4 instead of H_2S for n^+-layer doping	LD9918	Improved profile, but still not satisfactory. See Figs. 12 and 13. Postulate heavy n^+-doping, particularly with S causes profile problems. May be anomalous diffusion. Not understood.
A191-A200	Replaced Ga, recalibrated reactor.		
A201	n-layer on Cr-doped buffer layer	NK2912	Sharp interface. Hall data on n-layer $n(300) = 3x10^{16}$ cm^{-3}; (300) = 5512 $cm^2v^{-1}s^{-1}$. $n(77) = 2.5x10^{16}$ cm^{-3}; (77) - 16,800 $cm^2v^{-1}s^{-1}$.
A202	n^+-n-Cr buffer FET structure using Si as n^+ dopant.	NK2912	Buffer layer shows conducting knee.

SECTION III

MATERIAL CHARACTERIZATION

A. INTRODUCTION

The detection and identification of deep levels in high resistivity GaAs is an important step toward characterization of the material. Cr, Fe, and O are the most common elements used for producing deep states. Some investigators believe that both Cr and O are necessary to produce SI GaAs [5]. "Cr-free" undoped GaAs has also been reported [6]. The analytical detection of the elements causing deep levels is difficult, particularly in thin layers; for example, the Cr concentration in typical Cr-doped SI GaAs layers remains in the parts-per-million level. To date we have found that only spark-source mass spectroscopy (SSMS) has reliably detected Cr in GaAs.

This effort was directed towards characterizing SI GaAs, both in bulk form, as purchased from various vendors, and in epitaxial Cr-doped and "undoped" layers grown by CVD. (Undoped GaAs refers to high resistivity epi-layers grown by the mole fraction control method using the $AsCl_3/Ga/H_2$ process and layers grown by the $AsH_3/Ga/HCl$ process without intentional addition of dopants). A major objective was to develop a characterization method which would allow the evaluation of thin epi layers grown on SI GaAs substrates. Two methods were evaluated, namely, measurement of room temperature photoconductive response and Van der Pauw measurements. These are now described.

B. ROOM TEMPERATURE PHOTOCONDUCTIVITY

1. Introduction

It has been known for some time [7-9] that transitions to and/or from Cr acceptors in SI GaAs could be excited optically with a photon energy of about 0.9 eV. It is not clear in the literature whether holes or electrons are responsible for the increased photoconduction with this subgap illumination, although this could be determined with a photo-Hall experiment. Nevertheless, a peak in the photoconductive spectral response at 0.9 eV appears to be the "signature" of Cr presence in the lattice.

The measurement of photoconductivity as a function of photon energy was carried out using a Bausch and Lomb grating monochromator with appropriate filters. Measurements involving optical excitation are, in general, sensitive not only to the incident wavelength, but also to the intensity of the radiation. Since the output curve of the monochromator/filter combination is not independent of the wavelength, the system has to be calibrated. The need to employ filters to remove higher order grating modes usually enhances intensity variations as a function of wavelength. There are two available options:

a. Normalize the measured dependent variable to the intensity of radiation. For example, the photoconductivity is normalized to μW of incident radiation. This assumes implicitly that the measured parameter varies linearly with intensity. This is not always true; even simple photoconductivity can vary sub- or super-linearly with excitation intensity depending upon the position of the quasi-Fermi level with respect to traps, etc.

b. Change the monochromator exit slit setting to produce the same intensity al all wavelengths. Changing slit settings, however, effects spectral purity which may not be reproducible. This can cause problems particularly in the vicinity of sharp quantum transitions such as the band edge.

The procedure used in most of our measurements was option a; however, some measurements were made using option b. The corrections and slit setting for various monochromator/filter combinations were determined using a tungsten source and a calibrated thermopile.

2. Photoconductivity Measurements

a. SI Substrates - Photoconductivity measurements were made using square samples with alloyed In (or Sn) ohmic contacts at the four corners. This is a typical Van der Pauw configuration used for resistivity and Hall mobility measurements. The ohmic contacts were shielded from the incident radiation. Since the sample impedances are high, a special circuit was designed and built to allow measurement. Using IC op-amps (CA3130), the differential sample voltage was converted to a single ended signal at unity voltage gain and an input impedance of greater than 10^{12} ohm.

Figure 14 shows the room temperature (300 K) photoconductive response of three bulk grown substrates. The conductivity per μW of incident radiation is plotted as a function of photon energy. Note the evolution of a peak at 0.9 eV as the Cr content increases. The Cr content was measured by SSMS.

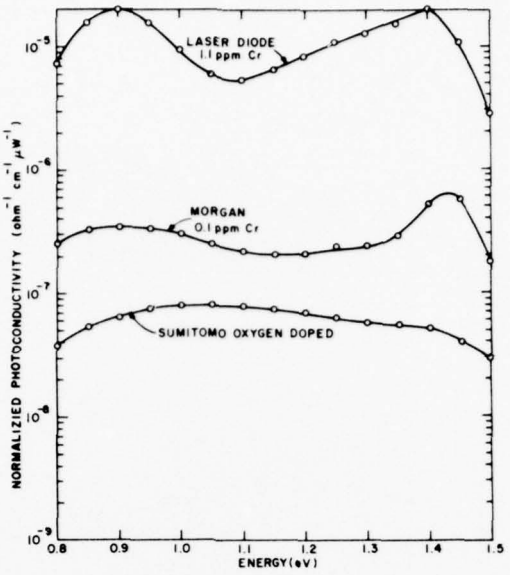

Figure 14. Room temperature photoconductivity response of SI GaAs substrate. Note evolution of a peak at ∿0.9 eV as Cr-content increases.

The Sumitomo* oxygen-doped substrate served as a control in the experiment. The PC response of this material is somewhat featureless at 0.9 eV, as expected. The Morgan** substrate did show evidence of a peak at 0.9 eV. SSMS determined that the concentration of Cr in this sample was about 0.1 ppma-(2.3×10^{15} cm^{-3}). The Laser Diode† material exhibits a definite peak at 0.9 eV and was determined, by SSMS, to have a Cr concentration of about 1.0 ppma-(2×10^{16} cm^{-3}). In addition, the Laser Diode material showed lower dark conductivity than the Morgan and had the slow photoresponse characteristic of a high concentration of deep traps.

Figure 15 shows the photoconductive response of two nominally (as specified by vendor) O-doped SI GaAs substrates. Note that the Sumitomo O-doped sample is featureless at 0.9 eV. while the Laser Diode O-doped sample appears to show a peak at 0.9 eV. Samples from these boules were also analyzed by SSMS. The Laser Diode sample shows a Cr concentration of 3.5×10^{16} cm^{-3} and an oxygen concentration of about 10^{16} cm^{-3}, while the Sumitomo sample shows

*Sumitomo Electric Industries, Ltd., Osaka, Japan.
**Morgan Semiconductor Inc., Garland, TX.
†Laser Diode Laboratories, Inc., Metuchen, NJ.

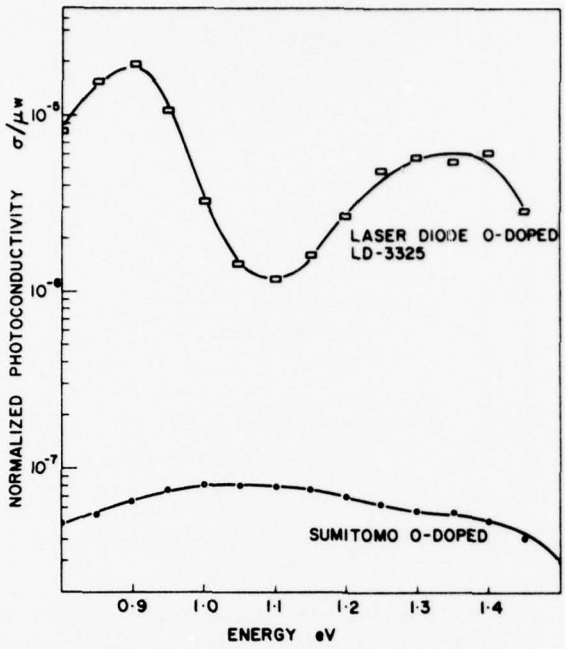

Figure 15. Photoconductive response of two nominally O-doped SI GaAs substrates.

$4x10^{16}$ cm^{-3} of Cr and $3x10^{16}$ cm^{-3} of O. The strikingly different photoconductive response of two wafers with similar Cr and O concentrations as measured by SSMS is not understood. It should be noted that O concentration measured by SSMS is somewhat uncertain. Both these substrates could withstand annealing at 850°C for 20 minutes in a hydrogen atmosphere without degradation of resistivity.

Figure 16 shows the room temperature photoconductive response of three Morgan semi-insulating GaAs substrates. Note that M_2 and M_4 have reasonably similar response with broad peaks at about 0.9 eV characteristic of Cr. Substrate M_1, on the other hand, shows different characteristics. SSMS measurements show Cr content of $<1.7x10^{15}$ cm^{-3} for M_1, $1.6x10^{16}$ cm^{-3} for M_2, and $2.5x10^{15}$ cm^{-3} for M_4. Under a high temperature anneal test (750°C, 30 mins.), M_2 did not show conversion to lower resistivity, some M_4 samples showed slight degradation, while M_1 samples degraded considerably.

Figure 17 is a replot of the photoconductive response of two Laser Diode substrates, one nominally O-doped (LD-3325) and the other Cr-doped (LD-9918). The responses are essentially similar. This is consistent with SSMS measurements which show Cr in both substrates.

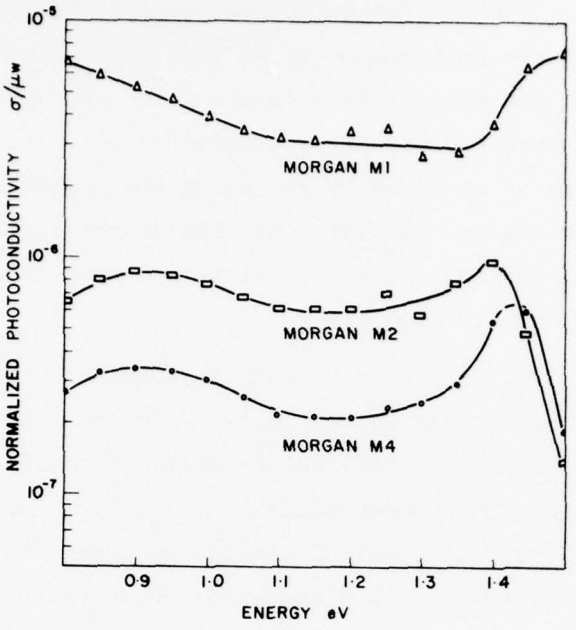

Figure 16. Photoconductive response of three Morgan Cr-doped SI GaAs substrates.

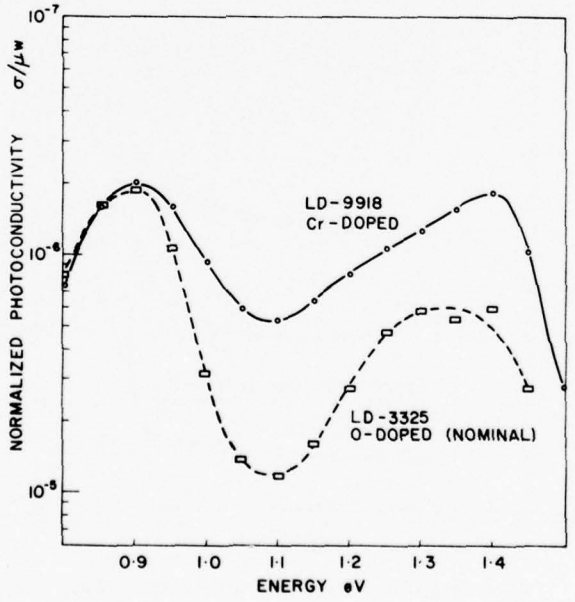

Figure 17. Nominally O-doped and Cr-doped SI GaAs substrates. Note similar photoconductive response.

We conclude that photoconductivity measurements can be used to non-destructively detect the presence of Cr in most SI GaAs substrates. The only discrepancy observed was the Sumitomo sample which was specified by the vendor as O-doped but SSMS detected significant amount of Cr. It is likely that other deep states can be resolved by extending the measurement to lower temperatures and photon energy. As yet, there is no correlation between other substrate properties such as ability to withstand high temperature ($\geq$750°C) anneals and photoconductive response.

b. High Resistivity Epi Layers on SI GaAs Substrates - Application of this method directly to the *in situ* detection of Cr in thin epi layers grown on SI GaAs substrates is not straightforward, however. Measurements of the optical absorption coefficient of Cr-doped material (Fig. 18) showed a negligible increase at 0.9 eV. Thus, the material remains optically transparent, and any increase in photoconductivity could come from the Cr-doped substrate as well as the buffer layer. In view of the relative thickness, it seems unlikely that the effects of the buffer layer at 0.9 eV would be seen at all.

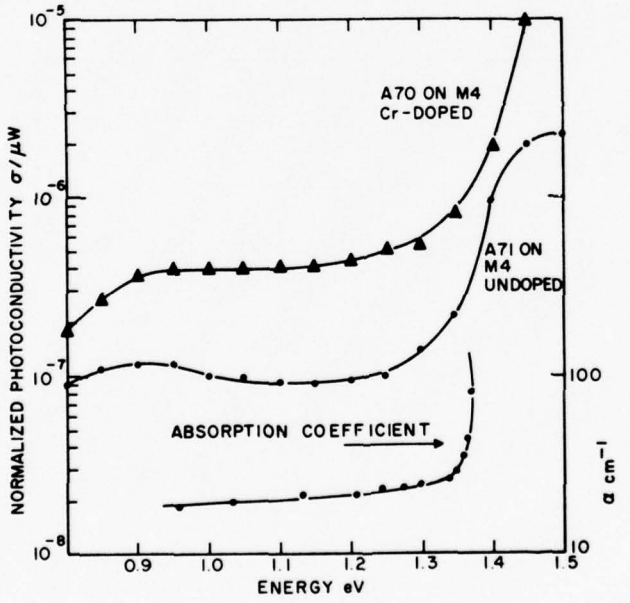

Figure 18. Photoconductive response of high resistivity epi layers on SI GaAs substrate (M4). Absorption coefficient plot also shown.

On the other hand, band-edge illumination is absorbed very rapidly with depth because of the large value of the absorption coefficient. Behavior of the photoconductive spectral response for the substrates tested was always similar. Conduction increased near the band-edge and then dropped off as the photon energy increased (see Fig. 17). This is interpreted as being due to a large value of the surface recombination velocity S. As the generated hole-electron pairs are confined to the surface, the photoconductive is seen to decrease. Figure 18 shows the room temperature photoconductive spectral response for two SI epi films on the Morgan M_4 substrate. The characteristic dip above the band-edge seen for the substrate was not observed for either the undoped or Cr-doped samples indicating a lower value of S in the epi material. It is not known, however, whether this fact can be used to advantage in material characterization.

The behavior of the absorption coefficient α makes near-bandedge radiation a useful probe of variable depth into the sample. It is likely that photo-Hall measurements with near-band-edge illumination will allow one to electrically separate the effect of transport in the epitaxially grown high resistivity layers from transport in the bulk grown SI GaAs substrate. However, the significance of such photo-Hall data and their correlation to eventual device performance is as yet unknown.

The usefulness of photoelectronic measurements with subgap and bandgap radiation in characterizing GaAs:Cr has become apparent. Future effort will be directed toward lowering measurement temperatures for a better resolution of deep levels.

C. RESISTIVITY MEASUREMENTS

Another basic transport study was the measurement of the resistivity of several SI GaAs substrates and substrate epilayer structures as a function of temperature. Extensive measurements of the resistivity-temperature characteristics of GaAs have been recently reported by investigators at Rockwell International [5]. The measurements reported here are similar but on substrates from different vendors.

The resistivity measurements were made using square Van der Pauw samples with Sn contacts as described in Section III, paragraph B. Similar instrumentation was used. Where possible, the Hall mobility was computed assuming single carrier transport. The temperature range under investigation was from 27°C to 170°C. The Sn ohmic contacts were covered by silver epoxy to prevent oxidation and subsequent powdering at elevated temperatures. These measurements were carried out in the dark to avoid effects of photo-generated carriers.

In order to meaningfully interpret the resistivity-temperature characteristic, it is desirable to remove the implicit temperature dependence of the density of states and the various donor and aceeptor energy levels. The procedure used by Zucca has been employed [5]. The function $\rho T^{1.5}$ has been plotted as a function of $1/T'$. Since the density of states is proportional to $T^{1.5}$, plotting $\rho T^{1.5}$ removes this implicit temperature dependence. T' is a modified temperature given by:

$$T' = T \frac{E_g\ (300K)}{E_g(T)} \tag{1}$$

where $E_g(T)$ is the energy gap at a temperature of T (Kelvin). This assumes that relative energies of the impurity levels are proportional to the energy gap. Instead of correcting energies for thermal variations, the correction is made on kT since the energy differences are always divided by kT in expressions for resistivity [5].

The energy gap of GaAs as a function of temperature was determined by the expression of Panish and Casey [10];

$$E_g(T) = 1.522 - 5.8\text{x}10^{-4} \frac{T^2}{T + 300}\ \text{eV} \tag{2}$$

where T is the temperature in degrees Kelvin. The parameter $1000/T'$ is plotted as a function of 1000/T in Fig. 19 over the temperature range of 300-500 K. In this temperature range we can thus approximate the value of $1000/T'$ by the following expression:

$$\frac{1000}{T'} = \frac{1100}{T} - 0.33 \tag{3}$$

Figure 20 is a plot of $\rho T^{1.5}$ as a function of $1000/T'$ for two samples from a lot of Morgan M4 substrates. A least square fit to the data is also shown.

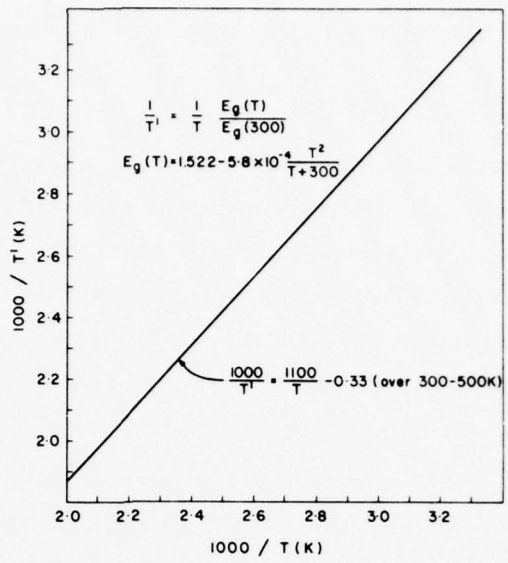

Figure 19. Plot of 1000/T´ as a function of 1000/T.

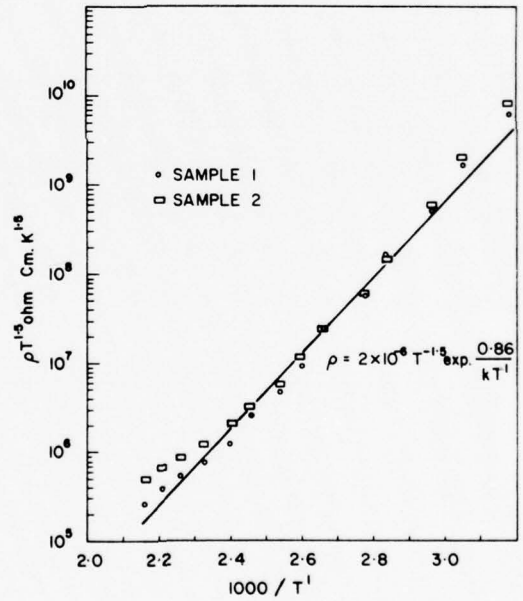

Figure 20. $\rho T^{1.5}$ as a function of 1000/T´ for Morgan M4 substrates.

Recall that this substrate has a Cr concentration of 0.1 ppma (2.2×10^{15} cm^{-3}). From the least square fit to the data, we can write the resistivity ρ as:

$$\rho = 2 \times 10^{-6} T^{-1.5} \exp\left(\frac{0.86}{kT'}\right) \tag{4}$$

The resistivity is thus thermally activated with an activation energy of about 0.86 eV. This assumes that the mobility μ is independent of temperature over this temperature range. This assumption is justified later.

Let us now compare this result to the measurements of Zucca for the low Cr (5×10^{15} cm^{-3}) case quoted in reference [5]. Zucca found that for the particular crystal under consideration:

$$\rho = 1.08\ T^{-1.5} \exp\left(\frac{0.72}{kT'}\right) \tag{5}$$

Zucca interprets this using the deep donor-deep acceptor model as containing an N_d/N_a of 14 and $E_c - E_d$ of 0.72 eV which corresponds to the O level in GaAs. For the Morgan substrate and the curve fit to the resistivity data (equation 4), we compute $E_c - E_a$ to be 0.86 eV which is in reasonable agreement to the depth of the Cr level of 0.84 eV reported in the literature [11]. Assuming an average mobility of 3000 $cm^2 V^{-1} s^{-1}$ and a degeneracy factor g_a of unity and using equation (12) of [15], we compute N_a/N_d to be 1.5.

Figure 21 is a plot of the Hall mobility of sample M4 from measured data assuming single carrier transport. The Hall constant was found to be well behaved and did not change sign over the measured temperature range of 300 to 500 K. Thus our assumption of a constant mobility of 3000 $cm^2 V^{-1} s^{-1}$ is a reasonable assumption for the calculation of N_a/N_d. Also note that this mobility-temperature characteristic is very similar to those reported by Lin for GaAs: Cr [12].

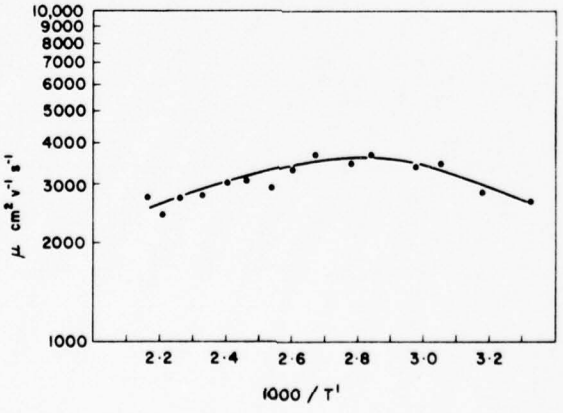

Figure 21. Hall mobility as a function of 1000/T′ for Morgan M4 substrate.

Figure 22 shows a similar plot of $\rho T^{1.5}$ as a function of 1000/T′ for a Nikkei-Kako* (NK), Cr-doped substrate from dark conductivity measurements. A straight line fit to these data indicate an activation energy of the order of 0.74 eV which is close to the O-level in GaAs (0.72 eV). However, it was not possible to measure Hall mobility because the Hall voltages were very small. Thus, the resistivity may be controlled by two levels, a deep donor and a deep acceptor. It may therefore be incorrect to associate the 0.74 eV number with oxygen and a more complex curve fit procedure as discussed by Zucca may be necessary [5]. In fact, other NK samples were found to be p-type at 27°C and became n-type above 50°C indicative of mixed conduction.

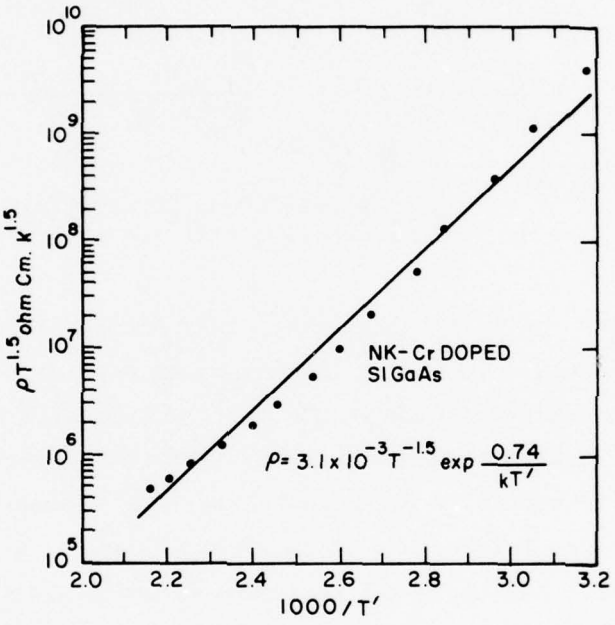

Figure 22. $\rho T^{1.5}$ as a function of 1000/T′ for NK SI GaAs substrate.

Note that for Morgan substrates, the activation energy of 0.86 roughly correlates with the broad peak at 0.9 eV seen in photoconductivity measurements.

Figure 23 shows the $\rho T^{1.5}$ - 1000/T′ charcateristics of the NK substrate repeated from the previous figure. The points, however, represent the data obtained from a dark conductivity measurement carried out on an undoped epitaxial

*Nikkei-Kako Company, Tokyo, Japan.

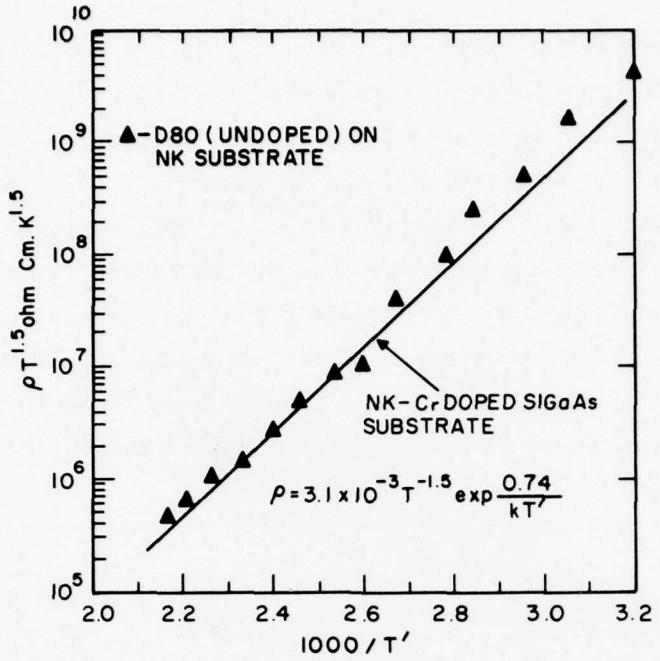

Figure 23. $\rho T^{1.5}$ data points for D80 on NK substrate. The straight line is the characteristic of the substrate alone.

SI layer (D80) grown on an NK substrate. This undoped layer was grown using the $AsCl_3/GaH_2$ process. The layer thickness was 6 μm and the substrate thickness 318 μm. Note that the data points for the composite structure fit reasonably well to the substrate characteristic. For these layer thicknesses, we can compute that ρ (buffer) $\geq$ 0.2 ρ (substrate) if we assume that the effect of the total layer resistance has to be about 10 times the substrate resistance to be unobservable. This puts a lower bound of 5×10^5 Ω-cm for the buffer layer resistance, which is adequate for device applications.

D. MISCELLANEOUS ANALYTICAL MEASUREMENTS

Various other methods for characterizing the Cr content in SI GaAs substrates and in Cr-doped epi layers grown on SI GaAs substrates were explored. As mentioned earlier, only SSMS could reliably detect Cr in SI GaAs substrates. Table 4 is a summary of SSMS measurements made during the course of this effect.

We also summarize our attempts at various analytical measurements for completeness.

TABLE 4. SPARK SOURCE MASS SPECTROSCOPY SUMMARY

	Cr cm^{-3}	O cm^{-3}	Si cm^{-3}	C cm^{-3}	Zn cm^{-3}	Comments
Morgan M5	5.4×10^{15}	2.2×10^{16}	3.1×10^{16}	2.2×10^{16}	7×10^{14}	No thermal conversion.
Morgan M2	1.6×10^{16}	1×10^{17}	3.4×10^{16}	5.4×10^{16}	$<2\times10^{15}$	No thermal conversion. Inconsistent implantation results.
Morgan M1	$<1.7\times10^{15}$	1.2×10^{17}	5.6×10^{16}	5.4×10^{16}	7.7×10^{15}	Severe thermal conversion.
Crystal Specialties 3761	6.1×10^{15}	4.1×10^{16}	NM	6×10^{16}	NM	No thermal conversion. Good for implantation. Results in high activation efficiency when implanted with Si.
Mitsubishi Monsanto G102 -22F	7.3×10^{15}	4×10^{16}	NM	1×10^{17}	NM	No thermal conversion - Ion implant behavior good; similar to crystal specialties.
Laser Diode 3325 Nominally O-doped (Vendor specification)	3.5×10^{16}	1×10^{16}	NM	NM	NM	More Cr than O. 300K Photoconductivity shows Cr-peak at ~0.9 eV.
Sumitomo Nominal O-doped	4×10^{16}	2.5×10^{16}	NM	NM	NM	More Cr than O. 300K photoconductive response featureless. Very stable thermally. Cannot get high implant activation efficiency.
Laser Diode 3301	3.8×10^{16}	1.3×10^{16}	NM	NM	NM	
Laser Diode 3331	5.6×10^{16}	1.3×10^{17}	NM	NM	NM	
A2508-undoped epi-layer	7.7×10^{15}	4.6×10^{17}	5.3×10^{17}	4.2×10^{16}	ND	Undoped high epi-layer. Spark may have penetrated substrate.
A96; Cr-doped epi-layer	$<4\times10^{15}$	4×10^{17}	NM	NM	NM	Unsatisfactory measurement.
A81; Cr-doped epi-layer	$<2\times10^{15}$	1×10^{17}	NM	NM	NM	Unsatisfactory measurement.
Nikkei Kako Substrates	--	--	--	--	--	Resistivity very high -- too high to spark. No thermal conversion. Hall measurement shows mixed conduction effects.

1. Secondary Ion Mass Spectroscopy (SIMS)

Attempts to measure the Cr profile in Cr-droped epi GaAs layers by SIMS were unsuccessful. The Cr concentration was below the sensitivity limit of our instrument. The minimum detection limit for Cr in our SIMS equipment is believed to be somewhat greater than 1 ppma which corresponds to 2.2×10^{16} cm^{-3} density.

2. Atomic Absorption Analysis

Several samples of SI GaAs substrates with and without Cr-doped epi-layers were sent to EMV Associates Inc.* for atomic absorption analysis. This attempt was also unsuccessful. The characteristic Cr-lines were masked by Ga lines. The following is an excerpt from their report.

> "We have completed a preliminary analysis of the two samples you submitted. The analytical scheme for the wafers was as follows. The mass of sample A (Cr doped) was determined and sample B (substrate) was crushed and weighed so that a blank of equal weight could be used. Both samples were placed in beakers with 10 ml of redistilled, concentrated nitric acid. The samples were gently refluxed for several hours. At first, bubbles were observed coming from the GaAs solids, indicating the release of a gas (As ?). After further refluxing, the solids were chalk white and fine grained (GaO?). The solution was evaporated to approximately 3 ml forming a slurry. The Cr analysis was attempted using flameless atomic absorption.
>
> "The slurry was delivered to the flameless atomizer with a 25 microliter Oxford pipette. The initial results were essentially identical for both samples, that is, a concentration of approximately 10 ppb. The spectrophotometer was run using background correction which theoretically substracts background absorption from total absorption, yielding the desired atomic absorption. In practice, however, this correction is applicable only when background is less than 0.5 absorbance units. The background absorption signal of the GaAs slurries was on the order of 2 absorbance units. This precluded the analysis of Cr unless the source of background could be separated from the Cr signal. A systematic procedure was used to volatize the Ga salt either before or after the Cr signal was obtained. The results were unsatisfactory indicating the 2 elements have similar atomization temperatures in this matrix. Although it may be possible to analyze for Cr by flameless atomic absorption, it is not a routine procedure and would therefore require considerable time to develop a satisfactory methodology: perhaps one involving a preliminary chemical separation.
>
> "A surface analysis technique currently being developed may be capable of this analysis. This technique, IBSCA (ion beam spectrochemical analysis) combines the surface spatial resolution of SIMS (secondary ion mass spectrometry) with the chemical sensitivity of OES (optical emission spectroscopy)."

*EMV Associates, Rockville, MD.

3. X-ray Fluorescence Spectroscopy

Several samples were sent to Princeton Gamma Tech[†] for x-ray fluorescence spectroscopy. This method was also unsuccessful.

4. Analysis of Epi Cr-doped Layers by SSMS

Attempts were made to analyze epi-layers with SSMS using a weak spark to prevent erosion to the substrate and only vaporize the epi-layer. The results were inconclusive. Examination of the spark-eroded samples showed slight penetration into the substrate. Keeping this fact in mind, the 18 μm Cr-doped epi-layer A96 showed a Cr concentration of 0.06 ppma (1.32×10^{15} cm^{-3}) and the 20 μm Cr-doped epi-layer of wafer A81 showed a Cr concentration of less than 0.17 ppma (3.7×10^{15} cm^{-3}).

5. High Resolution Photo Luminescence

Several samples of Cr-doped epi-layers were delivered to the Office of Naval Research. These samples were then sent to the Naval Research Laboratory for evaluation by high resolution photoluminescence measurements. No feedback has been obtained to date.

[†]Princeton Gamma Tech, Princeton, NJ.

SECTION IV

ION IMPLANTATION

A. INTRODUCTION

One of the major reasons for developing a technology for the epitaxial growth of SI GaAs is to use this layer as starting material for ion implantation. If high quality epitaxial SI GaAs layers can be consistently grown on a variety of commercial bulk-grown SI substrates, more reproducible results can be obtained by ion implantation. Currently, one has to go through elaborate qualifying procedures before ion implanting into bulk SI GaAs substrates. The activation efficiency, and hence the peak carrier concentration obtained for a given implant dose is currently a strong function of the quality of the substrate. Accordingly, we are investigating implantation of ^{32}S and ^{28}Si into epitaxial buffer layers and comparing the properties of the resulting layers with direct implantation into various SI GaAs substrates. This ion implantation effort is supported in part with Company funds.

B. SUBSTRATE QUALIFICATION

The substrate qualification procedure used is that reported in the literature [13]. Samples from substrate lots were bombarded with Ar ions at an energy of 200 keV and at a dose of $5x10^{12}cm^{-2}$ to simulate implant damage. The samples were then annealed under As overpressure at 800°C for 20 minutes. The resistance of a standard test pattern was measured before and after the bombardment/anneal procedure. Table 5 is a partial list of the substrates evaluated to illustrate typical results.

C. POST IMPLANT ANNEAL

The post-implant annealing of GaAs to remove implantation damage and activate the implanted species is generally difficult since GaAs tends to dissociate at the commonly used anneal temperatures of 800°-900°C. Dielectric encapsulation (SiO_2, Si_3N_4, AIN, etc.) has been used to prevent dissociation, but this often results in poor wafer surface due to out-diffusion of Ga or As into the encapsulant or uncontrolled in-diffusion into GaAs. This is

TABLE 5. SUBSTRATE QUALIFICATION

Wafer Number	Test Pattern Resistance Before Bombard/Anneal	Test Pattern Resistance After Bombard/Anneal	Comments
LD 9281	∿ 50 MΩ	∿1600 Ω	Unsuitable for implantation
LD 6917	∿ 50 MΩ	∿ 14 MΩ	Marginal
LD 10B	∿ 50 MΩ	∿ 30 MΩ	Suitable for implantation
LD 11B	∿ 50 MΩ	∿ 10 MΩ	Marginal
MA 193	∿ 50 MΩ	∿ 30 MΩ	Suitable for implantation
MA 201	∿ 50 MΩ	∿ 20 MΩ	Suitable for implantation
MA 196	∿ 50 MΩ	∿ 30 MΩ	Suitable for implantation

LD - Laser Diode Inc.
M - Morgan Semiconductor

particularly detrimental for the thin high-quality layers required for GaAs: FETs. *We have developed a method for annealing implanted wafers without encapsulation under arsenic overpressure. This procedure has been very sucessful and implanted wafers with excellent surface morphology have been obtained.*

D. RESULTS

Table 6 is a sample of results obtained on S-implantation to generate n- and n^+-layers. The first four rows describe implantation into epitaxial buffer layers (high resistivity) grown on SI GaAs substrates. *In general, implantation into epi-buffer layers leads to more consistency and superior mobility for a given carrier concentration.* The next four rows describe direct implantation into SI GaAs substrates. Note the greater variation in the results. Also note that when the substrate is of good quality (sample 45E), results comparable to implantation into epi-buffers are obtained. This substrate was cut from a specially qualified boule of GaAs. The final three rows are the results of increasing the implant dose to obtain n^+-layers for device contact regions. Figure 24 is a plot of the 300 K electron mobility of a number of implant runs. Theoretical curves for various compensation factors are also shown [14]. (The points are average Hall mobility while the theoretical curves are for drift mobility). Figure 25 is a plot of the average carrier concentration as a function of implant dose. Note the saturation at higher dose levels. *All implants*

TABLE 6. SULFUR IMPLANTATION

Sample No.	Substrate	Implant Energy (keV)	Implant Dose (cm^{-2})	Electron Mobility ($cm^2\ V^{-1}s^{-1}$)	Approx. Carrier Concentration (cm^{-3})	Comments
63B	Cr-doped epi-buffer on SI GaAs substrate	200	$5x10^{12}$	4053	$1.8x10^{17}$	Implantation in epi-buffers grown on SI Ga substrates.
10D	5 μm undoped epi-buffer on SI GaAs substrate	200	$5x10^{12}$	4005	$1.7x10^{17}$	
45A	3 μm undoped epi-buffer on SI GaAS substrate	250	$7x10^{12}$	4364	$1.4x10^{17}$	
45F	10 μm Cr-doped epi-buffer on SI GaAs substrate	250	$7x10^{12}$	4331	$1.2x10^{17}$	
62B	SI GaAs substrate; MM-G103	200	$4x10^{12}$	3318	$8.4x10^{16}$	Direct implantation into Si GaAs for n-layer
10A	SI GaAs substrate; LD	200	$5x10^{12}$	3220	$1.8x10^{17}$	
45E	SI GaAs substrate; MX	250	$7x10^{12}$	4067	$1.5x10^{17}$	
45D	SI GaAs substrate; LD8514B	250	$7x10^{12}$	3101	$1.1x10^{17}$	
64A	SI GaAs substrate; MMG102	200	$2x10^{13}$	2899	$5.8x10^{17}$	Direct implantation into SI GaAs for n^+-layers.
57	SI GaAs substrate; XS3761	200	$1x10^{14}$	3201	$1.5x10^{18}$	
50A	SI GaAs substrate; XS3761	200	$5x10^{14}$	2891	$1.7x10^{18}$	

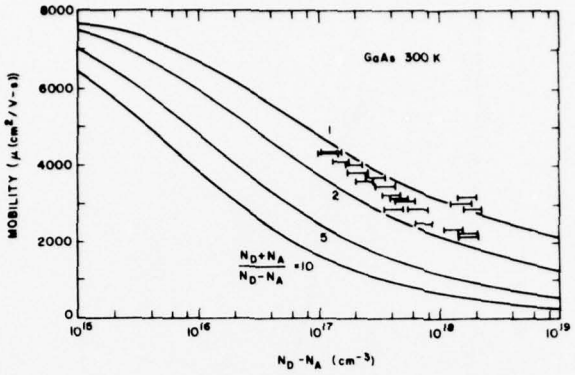

Figure 24. Electron mobility-carrier density plot for S implantation.

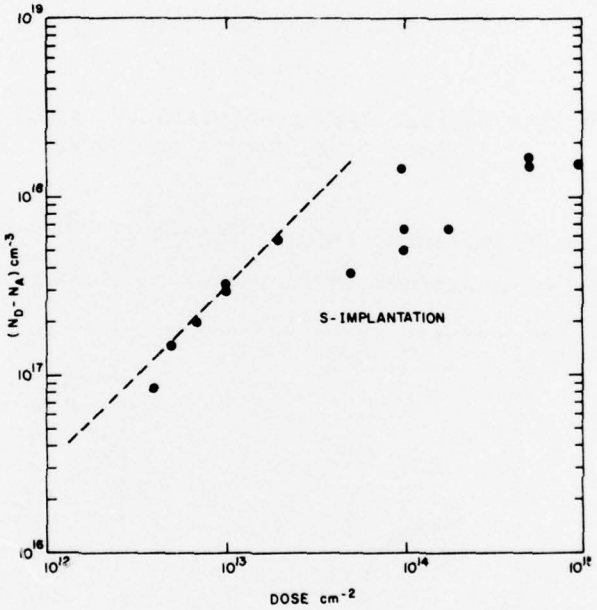

Figure 25. Carrier concentration as a function of dose for S-implantation.

were annealed without encapsulation under arsenic overpressure at 825°C for 20 minutes. The surface morphology of annealed wafers was excellent.

Table 7 summarizes the implantation of Si^{28} into GaAs, using the same format as in Table 6 and basically the same conclusions apply. The major difference between implantation of S and Si is that Si implanted layers are more reproducible and follow LSS theory more closely. Figure 26 shows typical carrier

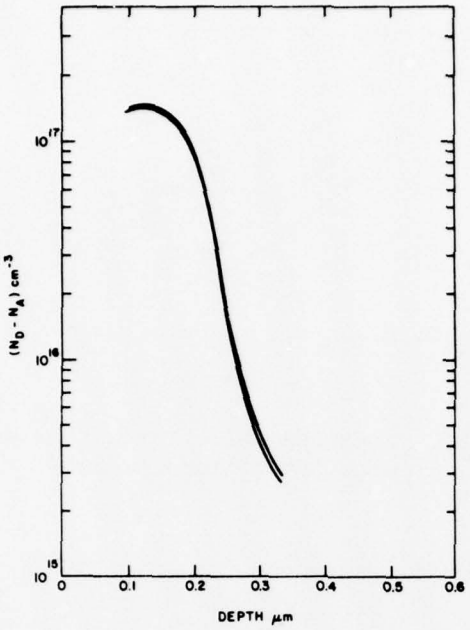

Figure 26. Carrier density profile for single Si implant $3.5 \times 10^{12} cm^{-2}$ at 200 keV.

density profiles of a Si implanted layer. Figure 27 is a profile of a double Si implant in a successful attempt to increase the surface doping density.

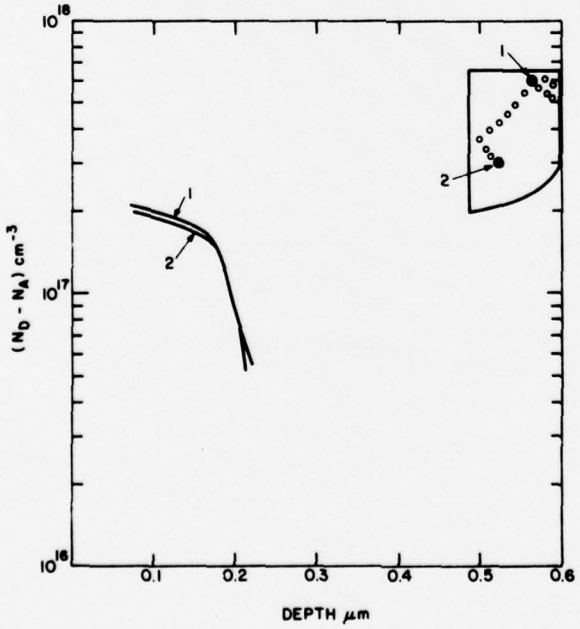

Figure 27. Carrier density profile for double Si implant. $1.5 \times 10^{12} cm^{-2}$ at 70 keV and $3 \times 10^{12} cm^{-2}$ at 200 keV.

TABLE 7. Si IMPLANTATION

Sample No.	Substrate	Implant Energy (keV)	Implant Dose (cm^{-2})	Electron Mobility ($cm^2\ V^{-1}s^{-1}$)	Approx. Carrier Concentration (cm^{-3})	Comments
A24A	6 μm undoped epi-buffer on SI GaAs substrate	200	$3x10^{12}$	4285	$8.2x10^{16}$	Implantation into epi-buffers.
A35D	5 μm undoped epi-buffer on SI GaAs substrate	200 70	$3x10^{12}$ $1.5x10^{12}$	4000	$1.9x10^{17}$	Double implant
A23A	5 μm Cr-doped epi-buffer on SI GaAs substrates	200	$4x10^{12}$	3928	$1.2x10^{17}$	
A286	SI GaAs substrate; XS3956F	200	$3.5x10^{12}$	4062	$2x10^{17}$	Direct implantation into SI GaAs for n-layer generation.
A3A	SI GaAs substrate; MM-G102	200	$4x10^{12}$	3570	$2x10^{17}$	
A4B	SI GaAs substrate; XS3956	200	$6x10^{12}$	3222	$1.9x10^{17}$	
A6	SI GaAs substrate; MM	200	$5x10^{13}$	2049	$1.1x10^{18}$	Direct implantation for n^+-layer generation.
A34	SI GaAs substrate; XS-3761F	200	$1x10^{14}$	2204	$1.1x10^{18}$	
A25	SI GaAs substrate; MM-G103	200	$3x10^{15}$	1909	$1.6x10^{18}$	

Figures 28 and 29 show the dose-carrier concentration and Hall mobility-carrier concentration and Hall mobility-carrier concentration characteristics, respectively.

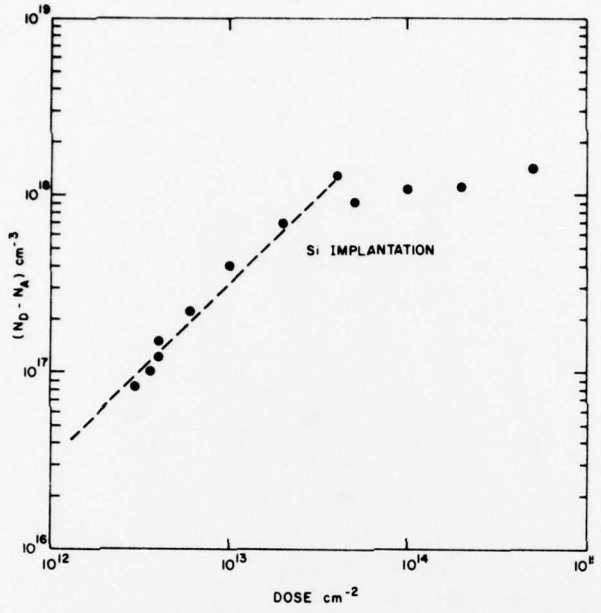

Figure 28. Carrier concentration as function of dose for Si implantation.

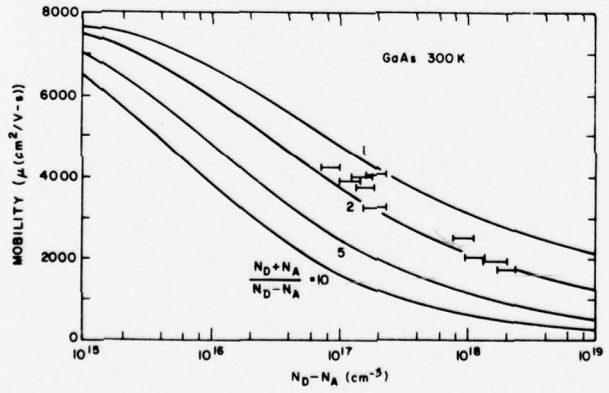

Figure 29. Electron mobility-carrier density plot for Si implantation.

SECTION V

PLANS FOR NEXT PHASE

1. We will continue epitaxial growth of high resistivity (>10^5 Ω-cm) layers using the $AsH_3/Ga/Cl_2/H_2$ system. Investigation of the use of metallic Cr and Fe will be emphasized.

2. The background (undoped) layers grown by the $AsH_3/Ga/Cl_2/H_2$ system are sometimes of high resistivity (10^4-10^6 Ω-cm). It is suspected that this phenomenon is due to out-diffusion of impurities or point defects from the substrate. While such layers can be used successfully as buffer layers, the control on their growth is poor. With our $AsCl_3/Ga/H_2$ VPE system, however, we can achieve background levels of $5x10^{14}cm^{-3}$ by adjusting $AsCl_3$ mole fraction. We will therefore add a Cr (and/or Fe) doping line to this system.

3. We will grow epitaxial Cr-doped layers on SI GaAs substrates from various manufacturers. We will attempt growth even on substrates proven unsuitable for expitaxy and/or ion implantation. The objective is to determine the extent to which epitaxial buffer layers can be used to overcome substrate deficiencies.

4. The implantation of donors (^{32}S and ^{28}Si) into high resistivity epitaxial layers grown on SI GaAs substrates will be investigated over the energy range of 100-2000 keV.

5. The annealing of implanted layers with high power pulsed laser radiation will be studied. Both sub-band gap (1.17 eV radiation using Nd:Glass) and above band gap (1.78 eV radiation using ruby) laser radiation will be evaluated for annealing.

6. We will grow n^+-n-n_B (buffer)-SI GaAs wafers for FET, TELD, and GaAs IC fabrication. FETs, TELDs and GaAs ICs will be fabricated in concurrent company and government sponsored programs. The results obtained will provide the ultimate operational evaluation of the technology being developed.

7. The development of photoelectronic methods to characterize high resistivity GaAs will be continued.

REFERENCES

1. S. T. Jolly et al. *Epitaxial Growth of Semi-Insulating GaAs*, Semiannual Report, March 1978, Control No. N00014-77-C-0542.

2. H. C. Huang, et al., "GaAs MESFET Performance,"*IEDM Dig.*, 1975, pp. 235-257.

3. A. Shibatomi, et al., "Characterization of Interface Region in VPE GaAs," *JCG Proc. Third Int. Conf. Vapor Growth and Epitaxy*, Aug. 1975.

4. H. M. Cox and J. V. DiLorenco, "Characteristics of an $AsCl_3/Ga/H_2$ Two-Bubbler GaAs CVD System for MESFET Applications," *Proc. Sixth Int. Symp. GaAs and Related Compounds;* Inst. Phys. Conf. Series, No. 33b, London, 1977, pp. 11-22.

5. R. Zucca, "Electrical Compensation in Semi-Insulating GaAs," Jour. Appl. Phys., 48, 5, May 1977, pp 1987-1994.

6. R. L. Henry and E. M. Swiggard, "LEC Growth of InP and GaAs Using PBN Crucibles," Proc. Sixth Int. Symp. GaAs and Relative Compounds, Inst. Phys. Conf. Series, 33b, London 1977, pp. 28-36.

7. D. R. Heath, P. R. Selway, and C. C. Tooke, "Photoconductivity and Infrared Quenching in Chromium-doped Semi-insulating Gallium Arsenide," Brit. J. Appl. Phys. (J. Phys. D) 1 (Ser. 2), 29 (1968).

8. W. Pleasiewicz, "Photoelectronic Investigations of Semi-Insulating p-Type GaAs:Cr Containing Neutral Chromium Acceptors," J. Phys. Chem. Solids 38, 1079 (1977).

9. H. J. Stocker, "A Study of Deep Impurity Levels in GaAs Due to Cr and O by AC Photoconductivity," J. Appl. Phys. 48, 4583 (1977).

10. M. B. Panish and H. C. Casey Jr., "Temperature Dependence of the Energy Gap in GaAs and GaP," Jour. Appl. Phys. 40, 1, Jan. 1969, pp. 163-167.

11. H. J. Stocker and M. Schmidt, "A Study of Deep Imparity Levels in GaAs," Jour. Appl. Phys., 47, 1976, p. 2450.

12. A. W. L. Lui, "Photoelectronic Properties of High Resistivity GaAs:O and GaAs:Cr Single Crystals," Ph.D. Thesis, Stamford University, 1975.

13. R. Zucca, et al., *Investigation of Technical Problems in GaAs*, Final Report, Contract No. F19628-75-C-0113, Feb. 1978.

14. D. L. Rode and S. Knight, "Electron Mobility in GaAs," Phys. Rev. 133, 1978, p. 2534.

DISTRIBUTION LIST

TECHNICAL REPORT

Contract N00014-77-C-0542

	number of copies
Program Management Defense Advanced Research Projects Agency Architect Building 1400 Wilson Blvd. Arlington, VA 22209	2
Code 427 Office of Naval Research Arlington, VA 22217	3
Naval Research Laboratory 4555 Overlook Avenue S.W. Washington, D. C. 20375	
Code 5220	1
Code 5270	1
Defense Documentation Center Building 5, Cameron Station Alexandria, VA 22314	12
ONR Boston 495 Summer Street Boston, Massachusetts 02210	1
TACTEC Battelle Memorial Institute 505 King Avenue Columbus, Ohio 43201	1
Dr. Y. S. Park AFAL/DHR Building 450 Wright-Patterson AFB, OH 45433	1
ERADCOM DELET-M Fort Monmouth, N.J. 07703	1
Texas Instruments M. S. 105 P. O. Box 5936 Dallas, Texas 75222	1

Mr. H. Cooke 1
Avantek, Inc.
3175 Bowers Avenue
Santa Clara, CA 95051

Mr. R. Bell, K 101 1
Varian Associates
611 Hansen Way
Palo Alto, CA 94304

Mr. R. Bierig 1
Raytheon Company
28 Seyon Street
Walthon, MA 02154

Mr. H. C. Nathanson 1
Westinghouse R&D Center
Beulah Road
Pittsburgh, Pennsylvania 15235

Dr. F. Blum 1
Rockwell International Science Center
P. O. Box 1085
Thousand Oaks, CA 91360

Mr. G. J. Gilbert 1
MSC
100 Schoolhouse Road
Somerset, New Jersey 08873

Mr. C. Krumn 1
Hughes Research Laboratory
3011 Malibu Canyon Road
Malibu, California 90265

Mr. Hunter Chilton 1
RADC/OCTE
Griffiss AFB NY 13441

Mr. Lothar Wandinger 1
ECOM/AMSEL/TL/IJ
Fort Monmouth, NJ 07003

Colonel Paul Mosteller 1
AFOSR/NE, Bldg 410
Bolling AFB Wash DC 20375

Dr. Harry Wieder 1
Naval Electronics Laboratory Center
Code 922
271 Catalina Blvd
San Diego, CA 92152

DISTRIBUTION LIST (Continued)

Dr. William Lindley
MIT
Lincoln Laboratory
E124A P. O. Box 73
Lexington, MA 02173

Mr. Sven Roosild
AFCRL/LQD
Hanscom AFB, MA 01731

Mr. John Kennedy
AFCRL/LQP
Hanscom AFB, MA 01731

Mr. Don Reynolds
AFAL/DHR
Wright-Patterson AFB, OH 45433

Mr. John Carroll
RADC/RBRP
Griffiss AFB, NY 13441

Dr. Robert Thomas
RADC/RBRM
Griffiss AFB, NY 13441